Journal of Drug Delivery Science and Technology 92 (2024) 105301

Contents lists available at ScienceDirect

Journal of Drug Delivery Science and Technology

journal homepage: www.elsevier.com/locate/jddst

Porous silicon microparticles as efficient carriers for immunologic adjuvants

Alessia Sambugaro [a,*], Marta Donini [b], Elena Chistè [a], Marina Scarpa [c], Stefano Dusi [b], Nicola Daldosso [a]

[a] Department of Engineering for Innovation Medicine, Fluorescence Laboratory, University of Verona, Strada le Grazie 15, 37134, Verona, Italy
[b] Department of Medicine, Division of General Pathology, University of Verona, Strada le Grazie 8, 37134, Verona, Italy
[c] Department of Physics, Laboratory of Nanoscience, University of Trento, Via Sommarive 14, 38123, Trento, Italy

ARTICLE INFO

Keywords:
Porous silicon
Pam3CSK4
Dendritic cells
Immunotherapy
Drug delivery

ABSTRACT

In this work we report a first-time combination of porous silicon (pSi) particles with the immunologic adjuvant Pam3CSK4, a TLR 1/2 agonist, as a tool for immunotherapy. pSi is a sponge-like biocompatible and biodegradable nanomaterial with high porosity, large surface-to-volume ratio and tunable surface, suitable for drug delivery applications. This study provides, by means of live-cell confocal microscopy, an insight about the time course of the interaction of free Pam3CSK4 vs vectorized by pSi microparticles with human dendritic cells (DCs). We found a delay in the ingestion of the agonist when carried by pSi microparticles. These findings were supported by the observation of the morphological changes related to the activation of DCs that occurred with a 5 h difference when treated with the vectorized ligand.

These results provide the first demonstration of pSi as a conceivable candidate to deliver Pam3CSK4 to DCs paving the way towards immunotherapy practice.

1. Introduction

Porous silicon [1] (pSi) is a sponge-like material having excellent prospects in the field of theranostics applications due to its interesting properties. First of all, it can be degraded into silicic acids and can be secreted by kidneys, thus it is biocompatible [2], it has been proved not to have toxicity effects to the cells and immune system activation. Secondly, it is characterized by a very high porosity [3,4] and intrinsic visible photoluminescence at room temperature [5,6]. These properties make porous silicon microparticles very promising as carrier for drug loading and release, to be traced both in vitro and in vivo by imaging. In recent years, silicon-derived materials have been thoroughly studied for applications in the field of theranostics: Sinha et al. combined the loading of gadolinium with the conjugation on the surface of an epidermal growth factor receptor to allow porous silicon nanoparticles as a carrier of MRI contrast agent targeting cancer cells [7]. Ferreira et al. developed a pSi nano-sized system able, on one hand, to target natriuretic peptide receptors expressed in cardiac fibroblasts, on the other, to deliver a novel hydrophobic cardioprotective drug capable to attenuate myocardial hypertrophic signalling and at the same time the chelation of ^{111}In-label to perform single-photon emission computed tomography (SPECT) imaging [8].

Porous silicon can be produced with a simple procedure of porosification of crystalline silicon wafers by electrochemical etching followed by fragmentation and particle size homogenization by ultrasounds. The resulting powder has an intense photoluminescence (PL) in the orange-red portion of the visible spectrum upon UV excitation [9,10]. This optical emission is, however, not stable: in fact, PL quenches upon interaction with organic solvents. Therefore, the introduction of carboxylic groups at the microparticles surface, upon hydrosilylation [11], allows the stabilization for years of pSi microparticles stored in ethanol. Beside the optical stabilization, this reaction is important for further surface modifications.

Even if stable in organic solvent as ethanol, for years, the pSi microparticles bearing carboxylic groups showed a fast PL quenching in biological media, such as water, and this is a big issue when dealing with

Abbreviations: pSi, porous silicon; PL, photoluminescence; PBS, phosphate buffer saline; DCs, dendritic cells; TLRs, toll-like receptors; Pam3CSK4, Palmitoyl-3-cysteine-serine-lysine-4.

* Corresponding author. Strada le Grazie 15, 37134, Verona, Italy.
E-mail address: alessia.sambugaro@univr.it (A. Sambugaro).

https://doi.org/10.1016/j.jddst.2023.105301
Received 31 August 2023; Received in revised form 19 December 2023; Accepted 21 December 2023
Available online 27 December 2023

biomedical applications. Therefore, we studied a PEGylation protocol to cover the pSi microparticles with an organic coating, by covalent attachment of PEG and chitosan [12], and a deposition protocol by atomic layer deposition (ALD) of a thin inorganic (TiO_2) layer, whose thickness is easily tunable [13]. Such coated pSi microparticles were proved to be stable for several months in PBS (phosphate buffer saline), not to be toxic to the cells and not activating their immune response [13].

As previously introduced, the high and adjustable surface-to-volume ratio is an interesting feature that makes pSi suitable for drug delivery purpose. Indeed, pSi microparticles can be considered efficient drug carriers with large loading capacity and slow release rate that could be varied as a function of the functionalization of the surface [14,15].

On the basis that immunotherapy supported by the administration of molecular adjuvants, is expected to become the mainstream strategy for many severe diseases, here we investigate the delivery of immunologic adjuvant. Immunotherapy is a medical treatment whose aim is to enhance the immune response to fight infections and cancer. It is well known that dendritic cells (DCs) play a fundamental role in the activation of the immune response. They are able to detect and engulf the foreign agents: subsequently, they undergo a maturation process which enables them to present the antigens to lymphocytes, thus inducing their activation [16–18]. Stimulated DCs also release several kinds of cytokines which orchestrate both innate and adaptive immune response [19]. This effect can be achieved in various ways, including the challenge of DCs with antigens as well as molecules able to increase their response, i.e. vaccine adjuvants [20,21]. For instance, DCs are isolated from the blood, stimulated by specific antigens and adjuvants, and then re-injected into the patient to trigger the immune reaction [22].

Several molecules have been employed to increase the effectiveness of immunotherapy. In particular, agonists able to engage Toll-like Receptors (TLR) are considered good adjuvants because of their ability to strongly stimulate the immune response. TLR are expressed by immune cells, including DCs, and recognize several structures expressed by pathogen microorganisms [23]. These structures are part of the so-called Pathogens Associated Molecular Pattern (PAMPs), whose binding by TLRs induces the ability of DCs to present antigens and to release cytokines which trigger both the innate and adaptive immune response. Therefore, a local or systemic administration of PAMPs is a good way to enhance the effects of a vaccine [24].

Palmitoyl-3-cysteine-serine-lysine-4 (Pam3CSK4), a synthetic lipopeptide which mimics the acylated amino terminus of bacterial LPS, is a member of PAMPs recognized by TLR1 and TLR2 [25,26]. These receptors are constitutively present on the surface and on the endosomes of DCs and their engagement leads to DCs activation and maturation [27]. In particular, the intracellular expression of TLR2 by human DCs was clearly demonstrated by Uronen-Hansson et al. by means of confocal microscopy and immunostaining techniques [28]. Therefore, Pam3CSK4 gained interest for the development of new adjuvants to be used in immunotherapy and, alone or in combination with other TLR agonists, has been employed to improve the vaccine efficiency [29].

However, the use of TLR ligands for medical purposes is hindered by their poor bioavailability and short half-life once infused into the patients [30]. Inclusion in carriers such as nanoparticles has been investigated as a way to stabilize and protect these molecules and to get an efficient and fast release. In particular, Pam3CSK4 has been encapsulated in PLA [31,32], PLGA [33–35], *N*-trimethyl chitosan [36] ARC4 and ARC7 [37] nanostructures to improve its efficiency in different experimental conditions. However, as far as we know, no reports are available about the association of Pam3CSK4 with mesoporous silicon nanostructures (pSi microparticles). This material is particularly indicated to carry adjuvant molecules because of its high loading capacity, its "tunable" surface chemistry, and absence of toxicity. Moreover, it can release the loaded molecules at a slow and controlled rate in biological media. Despite this, the use of pSi microparticles for the development of theranostics vaccines has been poorly addressed [38,39].

In this paper, we report the results of investigations aimed at exploring the application of pSi microparticles as vaccine adjuvant carriers with the perspective to use them for immunotherapy. As an adjuvant we have chosen Pam3CSK4 [27]. In fact, Pam3CSK4 is a small, positively charged toll-like receptor ligand able to infiltrate the porous structure and to interact with the negative charge of pSi microparticles. We investigated whether the loading of Pam3CSK4 within these particles might affect the interaction of the ligand with the monocyte-derived DCs. Bare pSi microparticles [11] and TiO_2-functionalized ones [13] were previously demonstrated to be incapable to induce apoptosis or necrosis on DCs for concentrations up to 100 μg/ml. Pam3CSK4 is known to not show any toxicity at the concentrations we used (i.e., 10 μg/ml) [40]. It is, therefore, more than reasonable to consider that their combination won't exert any toxic effects on DCs.

The loading within the pSi microparticles was assessed by means of optical microscopy and by confocal microscopy; for this reason, a fluorophore-labelled molecule was necessary, at least in the preliminary experimental part. We chose Pam3CSK4 labelled with tetramethyl rhodamine, hereafter named Pam3CSK4-R, with a very intense PL emission at 578 nm upon 555 nm excitation, to check and establish the procedures to infiltrate it within the fabricated pSi microparticles and to investigate its release in vitro and the interaction with DCs.

2. Materials and methods

All the reagents and solvents used for the pSi microparticles preparation and functionalization were purchased by Sigma-Aldrich. All aqueous solutions were prepared with ultrapure water obtained by using an ultrafiltration system (Milli-Q, Millipore) with resistivity above 20 MΩ cm. Porous silicon samples have been fabricated and characterized following the procedures already assessed in our laboratory [11], briefly summarized in the following.

2.1. pSi microparticles fabrication and carboxyl functionalization

The porosification of boron doped p-type Si wafers (<100> oriented, 10–20 Ω cm resistivity, University wafers, Boston MA) was obtained by electrochemical etching at constant current (80 mA/cm^2) in ethanol: hydrofluoric acid (16 %) solution in a PTFE cell for 15 min. After removing the porous silicon layer from the wafer surface, the procedure was repeated several times and the obtained powder was dispersed in toluene. The material was fragmented into microparticles by 20 min sonication in a thermal bath.

A light-driven hydrosilylation by acrylic acid in toluene under mild stirring at 50 °C for 2 h was performed to introduce carboxylic groups on the porous surface. The obtained solution was washed by centrifugation with ethanol several times and kept in ethanol.

2.2. pSi microparticles characterization

Size and ζ-potential of pSi microparticles were analysed at 25 °C with Dynamic Light Scattering (DLS) by ZetaSizer Nano ZS (ZEN3600, Malvern Instruments, Malvern, Worcestershire, UK) with a 633 nm laser beam. For size calculation, samples were sonicated for 15 min, diluted 10 times from the ethanol stock solution, measured three times and averaged. For ζ-potential, samples were dried in an oven at 50 °C and suspended in PBS buffer, sonicated for 15 min, measured three times and averaged. Data analysis was performed by ZetaSizer software (7.10).

The optical properties were analysed by a Horiba Jobin-Yvon Nanolog Spectrofluorometer (Nanolog/Fluorolog-3-2iHR320, Horiba-Jobin Yvon, USA), with a 450 W xenon lamp and PMT detector. The samples PL spectra were acquired by excitation at 350 nm, 3 nm slit size, 1200 g/mm density grating (blazed at 500 nm), 0.2 s integration time and with a 370 nm cut-off filter.

Confocal multiphoton microscopy (Leica-Microsystems, Wetzlar, Germany) was used to show the internalization of pSi microparticles

loaded with Pam3CSK4-R by DCs at 400X magnification by using the 63X oil immersion objective (1.25 NA). 15 z-stacks were acquired, and the maximum intensity projections (MIPs) were obtained by using the LAS-AF software (Leica- Microsystems). A drop of the suspension was deposited on a microscope glass slide and diluted by addition of 2-(*N*-morpholino) ethane sulfonic acid (MES) buffer. Time-lapse confocal imaging was performed by seeding and treating the cells in a 8-well μ-slide (Ibidi GmbH, Germany). The images were processed for brightness and contrast with Imaris (Bitplane).

Pore size and particles size were checked by Scanning Transmission Electron Microscopy (Thermo Scientific™ Talos F200S 200 kV S/TEM, Thermo Fisher Scientific Inc, USA), by deposition of a 5 μl drop of the sonicated sample on a TEM copper grid coated with an amorphous carbon film.

2.3. Loading of Pam3CSK4 and Pam3CSK4-R

A stock solution at a concentration of 100 μg/ml of Pam3CSK4 was prepared by adding endotoxin-free water and vortexing until complete solubilization. Different concentrations of Pam3CSK4 (5 μg/mL and 10 μg/mL) were obtained by diluting with 2-(*N*-morpholino) ethane sulfonic acid (MES) buffer (pH 5.8) and loaded within pSi microparticles by using an immersion method. After drying overnight in a 50 °C oven, to completely remove the ethanol, the pSi microparticles were added to prepared solutions of Pam3CSK4. The suspensions were then briefly sonicated to redisperse the microparticles and incubated overnight under mild rotation at room temperature to induce the loading. After that, the supernatant containing the non-loaded ligand was taken off and stored for further investigations, and the residual pellet with the loaded microparticles was resuspended by adding fresh water and washed 3 times by centrifugation to remove the free Pam3CSK4 and finally resuspended in PBS buffer (pH 7.4).

Pam3CSK4-R (used for optical characterization purpose only thanks to its labelling) was loaded following the same procedure. It is worth noting here that Pam3CSK4-R and the same non-labelled molecule have very similar molecular weight [41,42] and comparable density, therefore, it is legit to consider similar loading and release behaviours. Loading capacity (LC%) and encapsulation efficiency (EE%) were calculated by using:

$$LC\% = \frac{mass\ of\ loaded\ drug}{mass\ of\ loaded\ particles} \times 100$$

$$EE\% = \frac{mass\ of\ total\ added\ drug - mass\ of\ non\ loaded\ drug}{mass\ of\ total\ added\ drug} \times 100$$

The amount of Pam3CSK4-R was quantified by fluorescence spectroscopy (Nanolog/Fluorolog-3-2iHR320, Horiba-Jobin Yvon, USA), measuring PL maximum emission at 578 nm by exciting at 555 nm.

2.4. Pam3CSK4 release test in vitro

The release of the molecule was studied in PBS buffer (pH 7.4) by fluorescence spectroscopy. After the loading of Pam3CSK4-R on pSi microparticles, the sample was centrifuged, and dispersed in PBS with mild agitation. To obtain the unknown concentrations of Pam3CSK4-R at the defined times, the external standard method was performed by creating a calibration curve of known concentration of the lipopeptide. First, a calibration curve in the same medium of the release study (i.e., PBS) is needed to correlate the intensity of the rhodamine PL signal to its concentration; then, the amount of released molecules is obtained by collecting the supernatant at set times (20, 40, 60, 90 and 120 min), measuring its PL and replacing the removed supernatant with "fresh" PBS.

2.5. Dendritic cells preparation

Upon approval of the Ethical Committee and after written informed consent (Prot. no. 5626, February 2nd, 2012; Prot. n. 57182, October 16, 2019), buffy coats from the venous blood of normal healthy volunteers were obtained from the Blood Transfusion Centre of the University Hospital of Verona. Peripheral blood mononuclear cells were isolated by means of Ficoll-Hypaque and Percoll (Cytiva, Uppsala, Sweden) density gradients. To generate DCs, monocytes were cultured at 37 °C in 5 % CO_2 for 5–6 days at 1×10^6 ml in 6-well tissue culture plates (Greiner, Nürtingen, Germany) in RPMI 1640 medium, supplemented with heat-inactivated 10 % low endotoxin FBS, 2 mM L-glutamine and stimulated with 50 ng/ml GM-CSF and 20 ng/ml IL- 4 (Miltenyi Biotec). The final DCs population was 98 % $CD1a^+$ (HI149, Becton Dickinson, San Jose, CA, USA), as measured by FACS analysis.

3. Results and discussion

3.1. Fabrication and characterization of unloaded and Pam3CSK4-loaded pSi microparticles

Carboxyl-functionalized pSi microparticles resulted to have a porosity of 16 ± 5 nm and a size of 820 ± 510 nm and a ζ-potential of −35 ± 1 mV, as measured by DLS.

PL spectrum, reported in Fig. 1 (Fig. 1, A), shows a band maximum at about 675 nm by excitation at 350 nm (the peak at 390 nm and the peak at 700 nm, indicated by the asterisks, are correlated to the Raman effect of the water [43] and the second order of the excitation wavelength, respectively), the inset displays the PL emission of the sample under excitation by UV light. The introduction of carboxylic groups stabilized the samples and allowed to avoid the quenching of the photoluminescence. TEM image (Fig. 1, C) shows the sponge-like structure and the porosity of the sample. EDXS spectrum confirmed the silicon-nature of the sample and the presence of silicon oxides (Figure SI_1). Confocal images (Fig. 1, D) allowed to confirm the successful loading of Pam3CSK4-R within pSi microparticles. In fact, as shown in the images, the digital superimposition of the signals (panel I) coming from pSi microparticles (excitation at 405 nm, emission at 650 nm) (panel II) and from the rhodamine labelling of Pam3CSK4-R (panel III) is evident. To better highlight the merging of the two images, pSi microparticles signal was set up as green while Pam3CSK4-R was set up as red. The presence of red spots (Pam3CSK4-R) without any corresponding green point (pSi PL) can be attributed both by a partial release of Pam3CSK4-R in the medium and by the low signal intensity of pSi. Indeed, it should be reminded that the optical quantum yield is about 71 % for tetramethyl rhodamine in PBS buffer [44] and only a few % for pSi [45]. For the aim of this work, the intrinsic PL of pSi was exploited to confirm the loading of the labelled version of the selected ligand by exciting separately through two different channels: on one hand, the pSi microparticles (PL emission centered at 650 nm by excitation at 405 nm) and, on the other hand, the rhodamine labelling (PL emission centered at 566 nm by excitation at 543 nm). While the investigation (by time-lapse confocal imaging) of the time course of the cellular uptake by DCs was done by using only the excitation wavelength of Pam3CSK4-R (i.e., 543 nm). Therefore, when analyzing the time-lapse images, the PL of the pSi is negligible compared to that of rhodamine (quantum yield of about 2–3 % and 100 %, respectively) and indeed its emission was not detectable.

3.2. Quantification of loaded Pam3CSK4-R

After having confirmed the ability of our carrier to load Pam3CSK4, experiments with Pam3CSK4-R in two different concentrations (5 μg/mL and 10 μg/mL) were performed in MES buffer (pH 5.8) to find the best concentration ratio between the payload and the carrier in order to optimize the loading within the pores. The amount of loaded plus non-loaded Pam3CSK4-R was compared to the initial amount incubated with

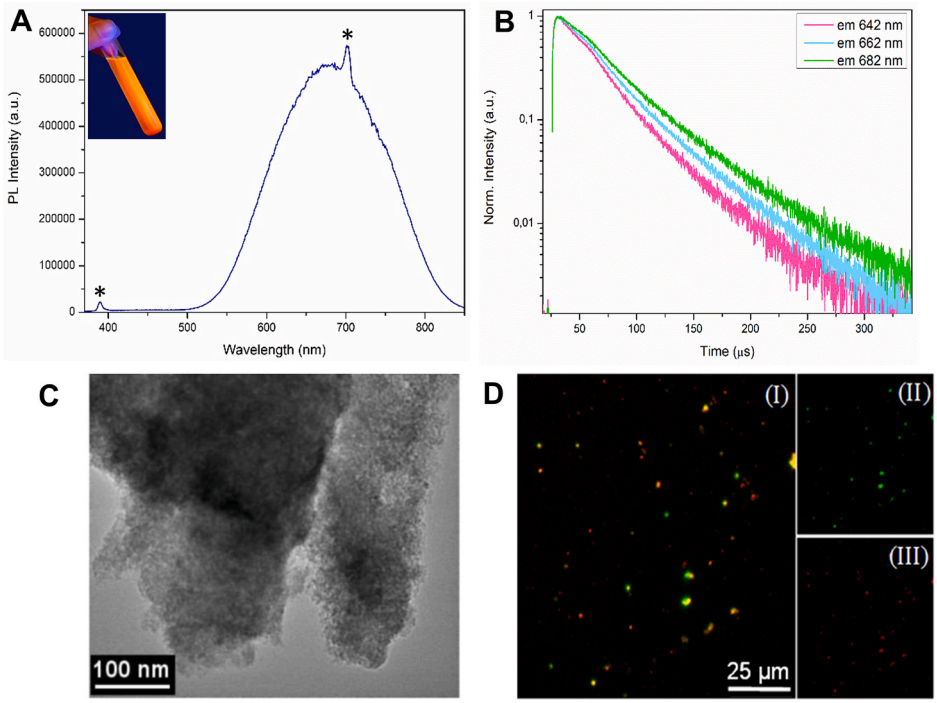

Fig. 1. Optical and structural characterization of a representative sample of pSi microparticles and loading confirmation of Pam3CSK4. (A) PL spectra under 350 nm excitation and (B) decay curves dependence on the emission wavelength by excitation at 350 nm. (C) TEM image of pSi microparticles (100 nm scale). (D) Confocal microscopy images of merged (panel I) and separate optical signals (panel II and III) of pSi microparticles, upon 405 nm excitation (green spots) and rhodamine, upon 543 nm excitation (red spots), respectively (25 µm scale). (For interpretation of the references to colour in this figure legend, the reader is referred to the Web version of this article.)

pSi particles to confirm the success of the quantification method.

Evaluation of loading capacity (LC%) and encapsulation efficiency (EE%) was conducted by quantification of the loaded Pam3CSK4-R and comparison with non-loaded Pam3CSK4-R by means of Fluorescence Spectroscopy (unknown concentration was determined by calibration curve of external standards).

The obtained loading capacity was 0.30 % for the sample with lower concentration and 0.49 % for the sample with higher concentration and the encapsulation efficiency was around 34 % for both of them. The non-linear dependence of the LC% on the drug concentration is consistent with the saturation of Pam3CSK4-R adsorption sites, as expected, since the loading capacity is dependent on the number of active sites as well as the material structure [46].

3.3. Release study of Pam3CSK4-R

The release profile of Pam3CSK4-R loaded pSi microparticles in PBS buffer was obtained by plotting the concentration of the released molecule as a function of time, as reported in Fig. 2 (the excitation and emission spectra of Pam3CSK4-R are shown in Figure SI_2). The unknown concentrations were obtained by using the calibration curve reported on the inset in Fig. 2.

The curve shows that after 20 min about 64 % of Pam3CSK4-R was released. After 40 min, 100 % reaching a plateau. This indicates that the molecule was not strongly bonded within the pSi pores, accordingly to the electrostatic nature of the binding between the carboxyl groups of the pSi and the amino groups of Pam3CSK4-R. The release rate plays a crucial role because it allows the encapsulated adjuvant to be not immediately accessible as the soluble one but, instead, by carrying it within our drug delivery system it's released in a relatively fast but continuous way. This is compatible with other findings about a similar system reported by Liu et al. regarding the release of drugs electrostatically bonded with pSi [47].

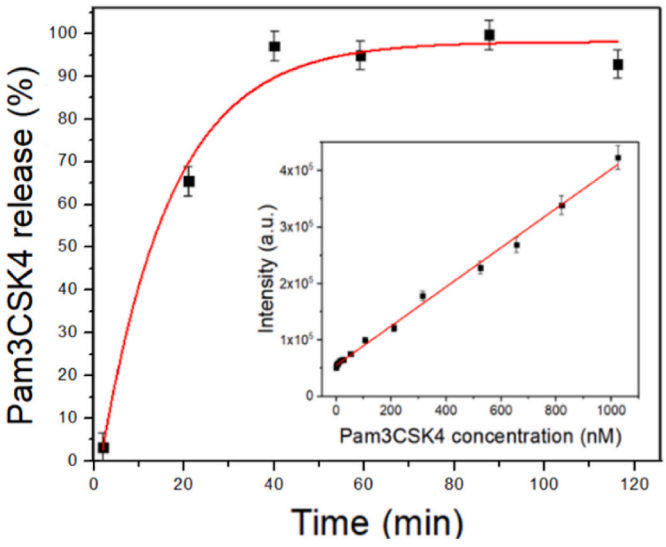

Fig. 2. Pam3CSK4-R concentration was measured at various times to determine the release rate. In the inset, the calibration curve to pass from rhodamine PL intensity to Pam3CSK4-R concentration is reported ($R^2 = 0.9944$).

3.4. Live-cell confocal imaging

To investigate the time course of the cellular uptake by human DCs of soluble Pam3CSK4-R vs Pam3CSK4-R carried by pSi microparticles, time-lapse confocal imaging was performed. In Fig. 3 are reported the confocal frames at 30 and 75 min captured with the red channel (excitation at 543 nm, emission at 566 nm) for DCs treated with soluble Pam3CSK4-R (left panels) and particles loaded with the same molecule (right panels).

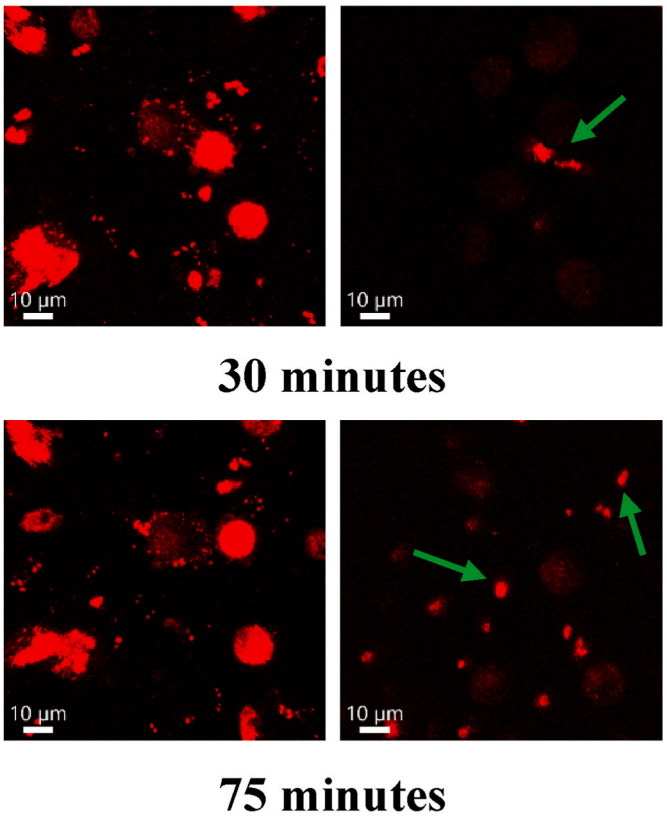

Fig. 3. Live-cell confocal images (543 nm laser excitation, frames at 30 and 75 min from the treatment) of DCs treated with soluble Pam3CSK4-R (left panels) and with pSi microparticles loaded with Pam3CSK4-R (right panels) (10 μm scale).

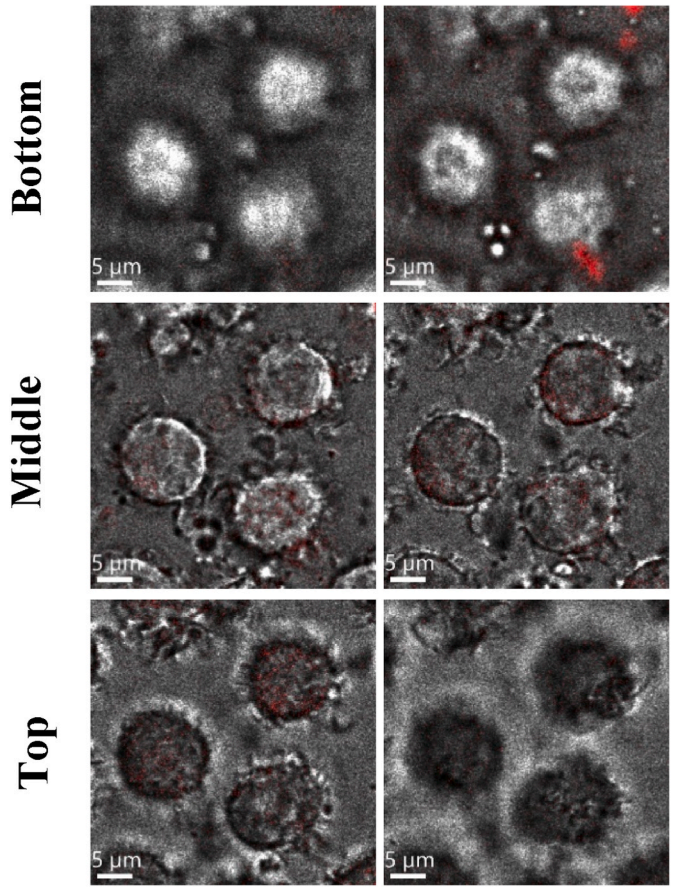

Fig. 4. Consequent stacks from the bottom to the top of the z-plane of a portion of a confocal image highlighting the presence of rhodamine-related signal inside the cells at 6 h (5 μm scale).

By analyzing the left panels (DCs incubated with free Pam3CSK4-R), it is evident that the red emission of the labelled TLR ligand was present in correspondence of the cells from the early beginning and it does not change significantly as a function of time: this suggests a sudden interaction with their receptors. On the contrary, when cells are treated with Pam3CSK4-R loaded within pSi microparticles (right panels of Fig. 3), the rhodamine red emission signal starts to be evident in the frame at 75 min. It is worth noting that an intense signal (large bright red spots indicated by green arrows) is present in all the frames, independently on the time, which is related to extracellular loaded-pSi particles not ingested by the DCs, probably because of their large dimensions (i.e., agglomerations of pSi microparticles). The presence of extracellular pSi microparticles was confirmed by the optical confocal images at the lowest slice along the z-axis, reported in Figure SI_3. By comparing the two images collected at 75 min, there is a clear difference between the intensity of the red signals in correspondence of the cells: for DCs incubated with loaded-pSi particles (right panels) the intensity of the signal is quite feeble compared to soluble Pam3CSK4-R (left panel). The latter, indeed, displays an analogous intensity with the extracellular loaded-pSi particles (indicated by green arrows in the right panel). This suggests the possibility of a delayed interaction between the TLR ligand and the receptors (beyond 1 h) when DCs are treated with the vectorized ligand instead of the soluble one. This time delay will be argued later in the manuscript.

To assess whether Pam3CSK4-R loaded-pSi microparticles were indeed internalized by DCs cells, as expected according to previous studies [13], we analysed optical image at different stacks on the z-plane. An example is shown in Fig. 4.

Moving from the lowest (bottom) to the highest (top) image on the z-plane, the rhodamine signal becomes more intense towards the middle and then decreases, stack by stack, while reaching the highest point, suggesting that the origin of the optical red signal is intracellular. Furthermore, at bottom and top of the z-plane, i.e., outside the cell, the only detected signal is due to the presence of some large extracellular particles.

To better analyze the time course of the particles ingestion we studied confocal images up to 15 h. The images reported in Fig. 5 clearly show that when DCs were treated with loaded-pSi particles the signal intensity from inside the cells gradually increased with the incubation time.

As the sequential confocal images suggest, when the Pam3CSK4-R is trapped inside the pores of the particles it might be not immediately accessible to the receptors of the cells leading to a slower display of the optical rhodamine signal. This hypothesis is supported by the results of Lamrayah et al. and by Alkie et al. [31,35], showing that when the DCs are incubated with free Pam3CSK4, the binding with the surface receptors happens instantly but just once. On the contrary, when Pam3CSK4 is transported by a carrier, the binding with the receptors is delayed presumably because the payload is mainly released in the endosomes after internalization of the drug delivery system.

TLR 2 are indeed constitutively expressed not only on the cellular membrane but also in the endosomes inside the DCs [28,48]. Therefore, we can reasonably suppose that when the DCs are treated with loaded-pSi particles there will be a first binding with the surface receptors of the small amount of ligand that is attached onto the external surface of the drug delivery system, that might justify the presence of a low intensity red signal during the first hours. Then, after going through endocytosis, the pSi particles release inside the cells the payload that would be able to repeatedly bind the TLR 2 located in the endosomes [28], hence the later display of an intense rhodamine signal.

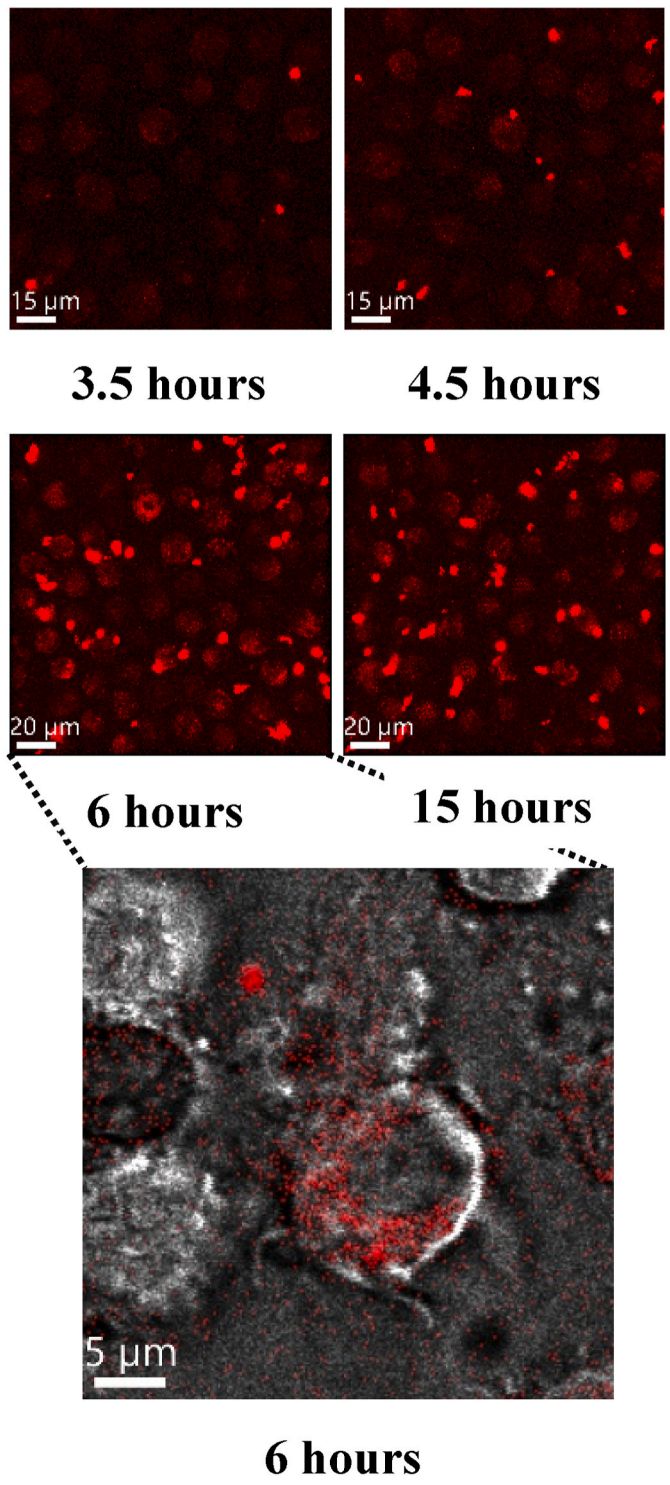

Fig. 5. Overnight frames (3.5, 4.5, 6 and 15 h after the treatment) of live-cell imaging of DCs treated with pSi microparticles loaded with Pam3CSK4-R displayed through the red channel (15 and 20 μm). A magnification of the 6 h image showing a DC treated with pSi microparticles loaded with Pam3CSK4-R and the signal distribution (5 μm scale) is illustrated in the bottom panel. (For interpretation of the references to colour in this figure legend, the reader is referred to the Web version of this article.)

We cannot however exclude that part of the extracellular loaded-microparticles might release their payload in the medium that would bind the surface receptors, although, according to the observations on the confocal images, it should be minority with respect to the intracellular release.

It is worth noting that after about 6–7 h apoptosys events increase because of the progression of time and the heating coming from the laser beam of the confocal microscope. Fig. 6 shows the confocal images with and without the overlap with BF, where it is clearly visibile the apoptosys diffusion over the time and the consequent decrease of cell confluence. It is appropriate to recap here that the apoptosys event cannot be attributed to the presence of the pSi particles since they do not show toxicity, as reported in Ref. [11].

Another interesting information from the analysis of the strong red optical signal inside the cells is that the molecule does not enter the nucleus, but it can be found spread into the cytoplasm. In the inset of Fig. 6 it is pictured the magnification of the frame, 6 h after the stimulation, to show the distribution of Pam3CSK4-R inside one representative cell. From the overlap between the BF image and the one obtained by excitation with the laser, it is clear that there is an absence of the red signal coming from the nucleus, instead, it is spread all over the cytoplasm and in the dendrites too.

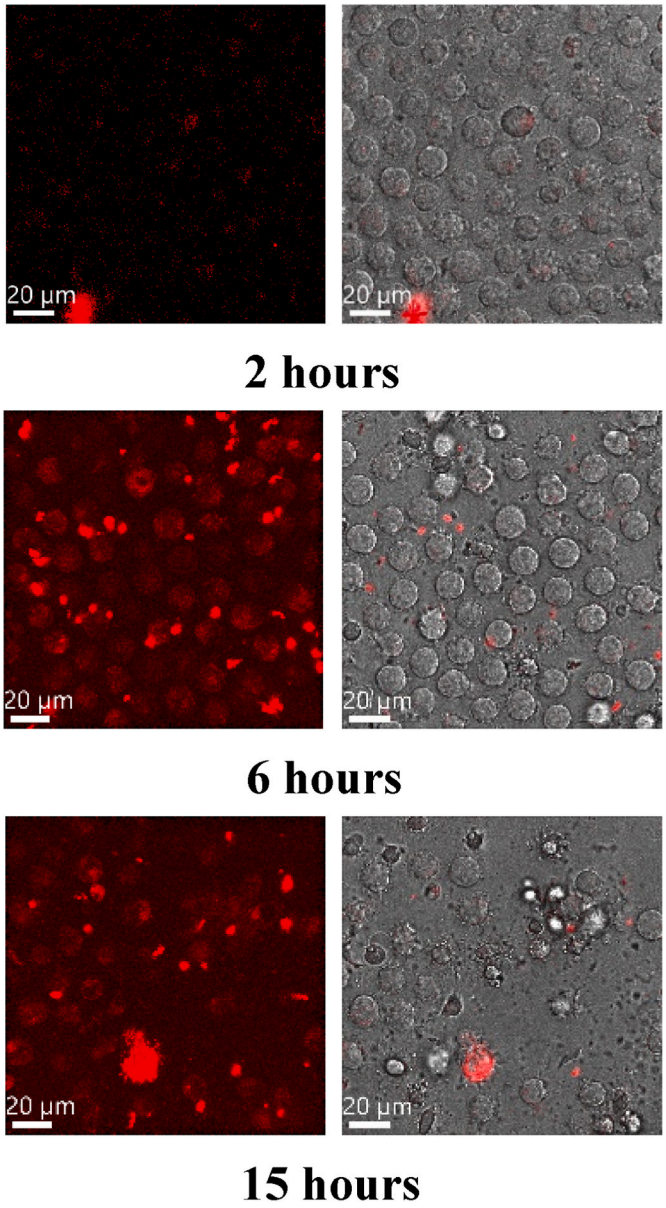

Fig. 6. Confocal images with (left) and without (right) the overlap with BF, where it is clearly visible the progression of the apoptosis events (at 2, 6 and 15 h, respectively (20 μm scale)).

Additional proof of the delayed ingestion caused by the loaded molecule compared to the soluble one can be found by observing the morphology of the DCs. As proposed by Xing et al. and by Verdijk et al. [49,50], DCs's transition from immature to mature condition is associated with morphological changes that are essential for the variation of the immunological functions related to the mature state, thus considering the modifications in the morphology as closely connected with the ability of DCs to activate the immune response. From their findings, when DCs are in their immature status they show a typical rounded shape with uniformly smooth cell surface. On the contrary, when the mature status is reached, their size becomes larger, the shape longer and flatter and the surface rougher. Moreover, they display longer protrusions (e.g., pseudopods, podosomes, filopodia, lamellipodia) and ruffles on the cell membrane.

Concerning the confocal images acquired during our experiments, DCs started to exhibit the morphological characteristics of the mature state (see Fig. 7) with a huge difference in terms of time in case they were stimulated with soluble Pam3CSK4-R, panel (A) or loaded within the pSi microparticles, panel (B).

In both cases DCs have a longer, larger and flatter form and they display protrusions and longer dendrites on their surface. Pam3CSK4 indeed when delivered by means of pSi microparticles preserves its ability to be taken up and to stimulate DCs and it is not endangered by the presence of the carrier. However: there is a 5 h' difference between the two images suggesting that a similar morphological structure, typical of the mature status, is achieved rather later when Pam3CSK4 is released from the pSi particles.

Fig. 8 shows that both untreated DCs (panel a) and DCs with bare pSi microparticles (panel c) are well distributed and round-shaped after 18 h, indicating that they are not stimulated. Differently, when treated with free Pam3CSK4 (panel b) and with loaded pSi microparticles (panel d), undergo a typical shape change, i.e., high elongation of their dendrites, after phagocytosis of the immunologic adjuvant.

4. Conclusions

In summary, we reported here for the first time the coupling of the immunologic adjuvant Pam3CSK4 with porous silicon microparticles and their interaction with DCs. The delivery of the TLR ligand via pSi microparticles allowed to maintain its ability to stimulate the DCs, but with a delay compared to the soluble ligand. By means of live-cell confocal imaging, we were able to follow the time course of cell internalization of the microparticles loaded with Pam3CSK4 and the increased presence of the adjuvant inside the cells by observing the red optical emission of the rhodamine optical label. Furthermore, a clear modification of the morphology of the stimulated DCs was observed at longer time (5 h delay). Studies regarding inorganic porous carriers, such as pSi, as delivery systems of molecules able to enhance the immune response (e.g., vaccine adjuvants) are very limited and mainly related to polymeric materials: consequently, the results reported here provide the first demonstration that pSi microparticles represent a good tool to deliver Pam3CSK4 to the DCs re-enforcing the path towards improved vaccine adjuvants by means of inorganic porous carriers. Future work will concern a detailed study of the release by DCs of cytokines involved in the activation of immune response with particular attention to the evolution with time. This, on one hand, would clarify the different behaviors that DCs show when Pam3CSK4 is delivered with or without pSi particles and, on the other, it would reinforce the improvement in efficacy when mediating the delivery with porous silicon carriers, as was proved here for the first time.

Funding

No financial support was provided for this work.

Author declaration template

I wish to confirm that there are no known conflicts of interest associated with this publication and there has been no significant financial support for this work that could have influenced its outcome.

I confirm that the manuscript has been read and approved by all named authors and that there are no other persons who satisfied the criteria for authorship but are not listed. I further confirm that the order of authors listed in the manuscript has been approved by all of us.

I confirm that we have given due consideration to the protection of intellectual property associated with this work and that there are no impediments to publication, including the timing of publication, with respect to intellectual property. In so doing I confirm that we have followed the regulations of our institutions concerning intellectual property.

The Corresponding Author is the sole contact for the Editorial process (including Editorial Manager and direct communications with the office). She is responsible for communicating with the other authors about progress, submissions of revisions and final approval of proofs.

CRediT authorship contribution statement

Alessia Sambugaro: Conceptualization, Data curation, Formal analysis, Investigation, Methodology, Writing – original draft. **Marta Donini:** Conceptualization, Data curation, Investigation, Methodology, Writing – original draft. **Elena Chistè:** Data curation, Investigation, Writing – original draft. **Marina Scarpa:** Conceptualization, Methodology, Validation, Writing – review & editing. **Stefano Dusi:** Conceptualization, Methodology, Validation, Writing – review & editing.

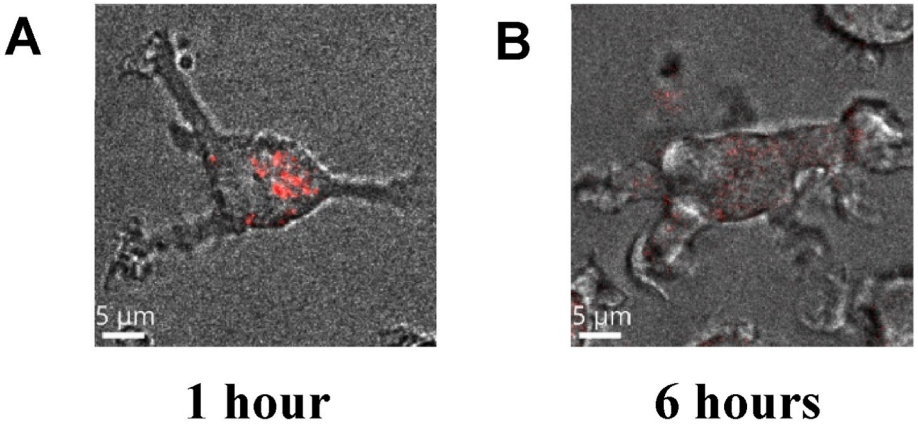

Fig. 7. Live-cell confocal images of DCs treated with (A) soluble Pam3CSK4-R and (B) with pSi microparticles loaded with Pam3CSK4-R (532 nm laser excitation, frames at 1 and 6 h, respectively) (5 µm scale).

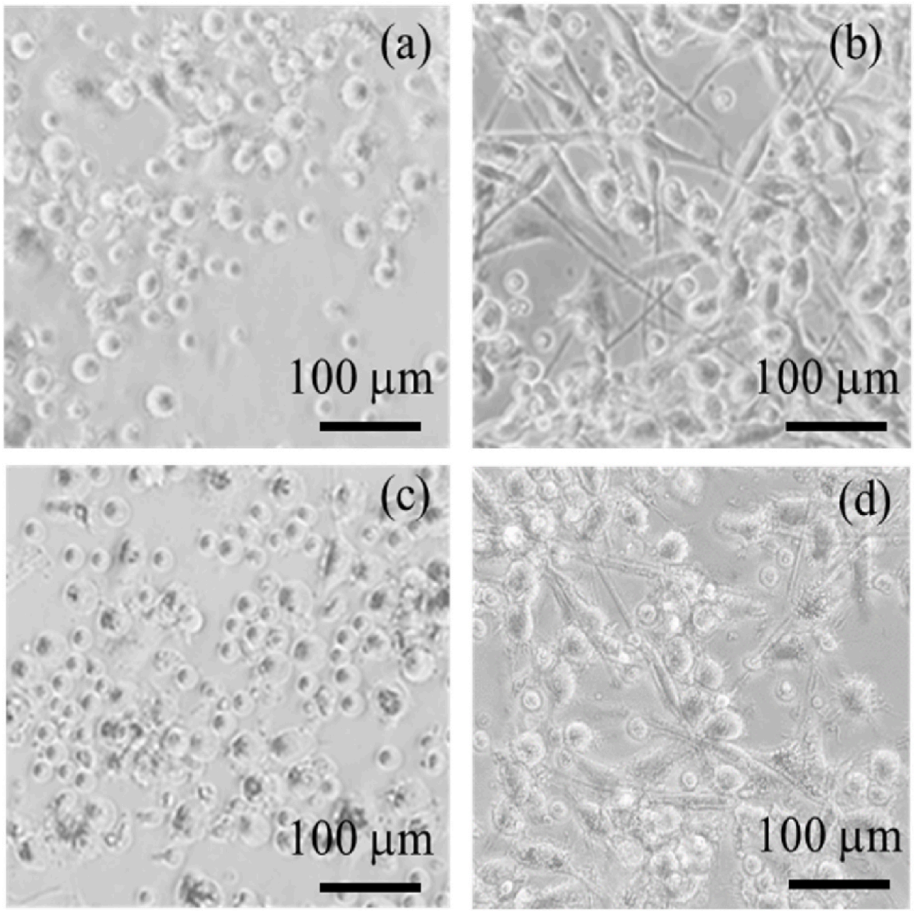

Fig. 8. Optical microscopy images of DCs. (a) untreated, (b) incubated (18 h) with free Pam3CSK4, (c) bare pSi microparticles, (d) pSi microparticles loaded with Pam3CSK4 (100 µm scale).

Nicola Daldosso: Conceptualization, Funding acquisition, Methodology, Project administration, Supervision, Writing – review & editing.

Declaration of competing interest

The authors declare that they have no known competing financial interests or personal relationships that could have appeared to influence the work reported in this paper.

Data availability

No data was used for the research described in the article.

Acknowledgements

Authors acknowledge CPT (Centro Piattaforme Tecnologiche) of the University of Verona for the access and support to the instrumentations.

Authors are grateful to G. Ischia, Department of Industrial Engineering, University of Trento, for the acquisition of TEM images.

Appendix A. Supplementary data

Supplementary data to this article can be found online at https://doi.org/10.1016/j.jddst.2023.105301.

References

[1] L.T. Canham, Silicon quantum wire array fabrication by electrochemical and chemical dissolution of wafers, Appl. Phys. Lett. 57 (1990) 1046–1048, https://doi.org/10.1063/1.103561.

[2] I.I. Slowing, J.L. Vivero-Escoto, C.-W. Wu, V.S.-Y. Lin, Mesoporous silica nanoparticles as controlled release drug delivery and gene transfection carriers, Adv. Drug Deliv. Rev. 60 (2008) 1278–1288, https://doi.org/10.1016/j.addr.2008.03.012.

[3] C.-F. Wang, M.P. Sarparanta, E.M. Mäkilä, M.L.K. Hyvönen, P.M. Laakkonen, J. J. Salonen, J.T. Hirvonen, A.J. Airaksinen, H.A. Santos, Multifunctional porous silicon nanoparticles for cancer theranostics, Biomaterials 48 (2015) 108–118, https://doi.org/10.1016/j.biomaterials.2015.01.008.

[4] R.J. Martín-Palma, V. Torres-Costa, Microscopy of porous silicon, in: L. Canham (Ed.), Handbook of Porous Silicon, Springer International Publishing, Cham, 2014, pp. 413–421, https://doi.org/10.1007/978-3-319-05744-6_41.

[5] J.-H. Park, L. Gu, G. von Maltzahn, E. Ruoslahti, S.N. Bhatia, M.J. Sailor, Biodegradable luminescent porous silicon nanoparticles for in vivo applications, Nat. Mater. 8 (2009) 331–336, https://doi.org/10.1038/nmat2398.

[6] E. Secret, M. Maynadier, A. Gallud, A. Chaix, E. Bouffard, M. Gary-Bobo, N. Marcotte, O. Mongin, K.E. Cheikh, V. Hugues, M. Auffan, C. Frochot, A. Morère, P. Maillard, M. Blanchard-Desce, M.J. Sailor, M. Garcia, J.-O. Durand, F. Cunin, Two-photon excitation of porphyrin-functionalized porous silicon nanoparticles for photodynamic therapy, Adv. Mater. 26 (2014) 7643–7648, https://doi.org/10.1002/adma.201403415.

[7] S. Sinha, W.Y. Tong, N.H. Williamson, S.J.P. McInnes, S. Puttick, A. Cifuentes-Rius, R. Bhardwaj, S.E. Plush, N.H. Voelcker, Novel Gd-loaded silicon nanohybrid: a potential epidermal growth factor receptor expressing cancer cell targeting magnetic resonance imaging contrast agent, ACS Appl. Mater. Interfaces 9 (2017) 42601–42611, https://doi.org/10.1021/acsami.7b14538.

[8] M.P.A. Ferreira, S. Ranjan, S. Kinnunen, A. Correia, V. Talman, E. Mäkilä, B. Barrios-Lopez, M. Kemell, V. Balasubramanian, J. Salonen, J. Hirvonen, H. Ruskoaho, A.J. Airaksinen, H.A. Santos, Drug-loaded multifunctional nanoparticles targeted to the endocardial layer of the injured heart modulate hypertrophic signaling, Small 13 (2017), 1701276, https://doi.org/10.1002/smll.201701276.

[9] J.R. Henstock, L.T. Canham, S.I. Anderson, Silicon: the evolution of its use in biomaterials, Acta Biomater. 11 (2015) 17–26, https://doi.org/10.1016/j.actbio.2014.09.025.

[10] V. Parkhutik, Porous silicon—mechanisms of growth and applications, Solid State Electron. 43 (1999) 1121–1141, https://doi.org/10.1016/S0038-1101(99)00036-2.

[11] N. Daldosso, A. Ghafarinazari, P. Cortelletti, L. Marongiu, M. Donini, V. Paterlini, P. Bettotti, R. Guider, E. Froner, S. Dusi, M. Scarpa, Orange and blue luminescence emission to track functionalized porous silicon microparticles inside the cells of the human immune system, J. Mater. Chem. B 2 (2014) 6345–6353, https://doi.org/10.1039/C4TB01031K.
[12] A. Ghafarinazari, M. Scarpa, G. Zoccatelli, M.C. Franchini, E. Locatelli, N. Daldosso, Hybrid luminescent porous silicon for efficient drug loading and release, RSC Adv. 7 (2017) 6724–6734, https://doi.org/10.1039/C6RA27102B.
[13] E. Chistè, A. Ghafarinazari, M. Donini, V. Cremers, J. Dendooven, C. Detavernier, D. Benati, M. Scarpa, S. Dusi, N. Daldosso, TiO2-coated luminescent porous silicon micro-particles as a promising system for nanomedicine, J. Mater. Chem. B 6 (2018) 1815–1824, https://doi.org/10.1039/C7TB02614E.
[14] D.-X. Zhang, L. Esser, R.B. Vasani, H. Thissen, N.H. Voelcker, Porous silicon nanomaterials: recent advances in surface engineering for controlled drug-delivery applications, Nanomedicine 14 (2019) 3213–3230, https://doi.org/10.2217/nnm-2019-0167.
[15] A. Nieto, H. Hou, S.W. Moon, M.J. Sailor, W.R. Freeman, L. Cheng, Surface engineering of porous silicon microparticles for intravitreal sustained delivery of rapamycin, Invest. Ophthalmol. Vis. Sci. 56 (2015) 1070–1080, https://doi.org/10.1167/iovs.14-15997.
[16] K.L. Hilligan, F. Ronchese, Antigen presentation by dendritic cells and their instruction of CD4+ T helper cell responses, Cell. Mol. Immunol. 17 (2020) 587–599, https://doi.org/10.1038/s41423-020-0465-0.
[17] D.A. Anderson, C.-A. Dutertre, F. Ginhoux, K.M. Murphy, Genetic models of human and mouse dendritic cell development and function, Nat. Rev. Immunol. 21 (2021) 101–115, https://doi.org/10.1038/s41577-020-00413-x.
[18] Y. Wang, Y. Xiang, V.W. Xin, X.-W. Wang, X.-C. Peng, X.-Q. Liu, D. Wang, N. Li, J.-T. Cheng, Y.-N. Lyv, S.-Z. Cui, Z. Ma, Q. Zhang, H.-W. Xin, Dendritic cell biology and its role in tumor immunotherapy, J. Hematol. Oncol. 13 (2020) 107, https://doi.org/10.1186/s13045-020-00939-6.
[19] C. Hespel, M. Moser, Role of inflammatory dendritic cells in innate and adaptive immunity, Eur. J. Immunol. 42 (2012) 2535–2543, https://doi.org/10.1002/eji.201242480.
[20] R. Perret, S.R. Sierro, N.K. Botelho, S. Corgnac, A. Donda, P. Romero, Adjuvants that improve the ratio of antigen-specific effector to regulatory T cells enhance tumor immunity, Cancer Res. 73 (2013) 6597–6608, https://doi.org/10.1158/0008-5472.CAN-13-0875.
[21] O.S. Søgaard, N. Lohse, Z.B. Harboe, R. Offersen, A.R. Bukh, H.L. Davis, H. C. Schønheyder, L. Østergaard, Improving the immunogenicity of pneumococcal conjugate vaccine in HIV-infected adults with a toll-like receptor 9 agonist adjuvant: a randomized, controlled trial, Clin. Infect. Dis. 51 (2010) 42–50, https://doi.org/10.1086/653112.
[22] K. Palucka, H. Ueno, J. Banchereau, Recent developments in cancer vaccines, J. Immunol. 186 (2011) 1325–1331, https://doi.org/10.4049/jimmunol.0902539.
[23] H. Kumar, T. Kawai, S. Akira, Pathogen recognition by the innate immune system, Int. Rev. Immunol. 30 (2011) 16–34, https://doi.org/10.3109/08830185.2010.529976.
[24] H. Lu, TLR agonists for cancer immunotherapy: tipping the balance between the immune stimulatory and inhibitory effects, Front. Immunol. (2014) 5. https://www.frontiersin.org/articles/10.3389/fimmu.2014.00083. (Accessed 26 May 2023).
[25] M.S. Jin, J.-O. Lee, Structures of the toll-like receptor family and its ligand complexes, Immunity 29 (2008) 182–191, https://doi.org/10.1016/j.immuni.2008.07.007.
[26] T. Kawai, S. Akira, The role of pattern-recognition receptors in innate immunity: update on Toll-like receptors, Nat. Immunol. 11 (2010) 373–384, https://doi.org/10.1038/ni.1863.
[27] J.H. Sakamoto, A.L. van de Ven, B. Godin, E. Blanco, R.E. Serda, A. Grattoni, A. Ziemys, A. Bouamrani, T. Hu, S.I. Ranganathan, E. De Rosa, J.O. Martinez, C. A. Smid, R.M. Buchanan, S.-Y. Lee, S. Srinivasan, M. Landry, A. Meyn, E. Tasciotti, X. Liu, P. Decuzzi, M. Ferrari, Enabling individualized therapy through nanotechnology, Pharmacol. Res. 62 (2010) 57–89, https://doi.org/10.1016/j.phrs.2009.12.011.
[28] H. Uronen-Hansson, J. Allen, M. Osman, G. Squires, N. Klein, R.E. Callard, Toll-like receptor 2 (TLR2) and TLR4 are present inside human dendritic cells, associated with microtubules and the Golgi apparatus but are not detectable on the cell surface: integrity of microtubules is required for interleukin-12 production in response to internalized bacteria, Immunology 111 (2004) 173–178, https://doi.org/10.1111/j.0019-2805.2003.01803.x.
[29] G.M. Weir, M. Karkada, D. Hoskin, M.M. Stanford, L. MacDonald, M. Mansour, R. S. Liwski, Combination of poly I:C and Pam3CSK4 enhances activation of B cells in vitro and boosts antibody responses to protein vaccines in vivo, PLoS One 12 (2017), e0180073, https://doi.org/10.1371/journal.pone.0180073.
[30] S.G. Reed, M.T. Orr, C.B. Fox, Key roles of adjuvants in modern vaccines, Nat. Med. 19 (2013) 1597–1608, https://doi.org/10.1038/nm.3409.
[31] M. Lamrayah, F. Charriaud, S. Hu, S. Megy, R. Terreux, B. Verrier, Molecular modelling of TLR agonist Pam3CSK4 entrapment in PLA nanoparticles as a tool to explain loading efficiency and functionality, Int. J. Pharm. 568 (2019), 118569, https://doi.org/10.1016/j.ijpharm.2019.118569.
[32] S. Megy, S. Aguero, D. Da Costa, M. Lamrayah, M. Berthet, C. Primard, B. Verrier, R. Terreux, Molecular dynamics studies of poly(lactic acid) nanoparticles and their interactions with vitamin E and TLR agonists Pam1CSK4 and Pam3CSK4, Nanomaterials 10 (2020) 2209, https://doi.org/10.3390/nano10112209.
[33] A. Katebi, R. Varshochian, F. Riazi-rad, M. Ganjalikhani-Hakemi, S. Ajdary, Combinatorial delivery of antigen and TLR agonists via PLGA nanoparticles modulates Leishmania major-infected-macrophages activation, Biomed. Pharmacother. 137 (2021), 111276, https://doi.org/10.1016/j.biopha.2021.111276.
[34] R.A. Rosalia, L.J. Cruz, S. van Duikeren, A.T. Tromp, A.L. Silva, W. Jiskoot, T. de Gruijl, C. Löwik, J. Oostendorp, S.H. van der Burg, F. Ossendorp, CD40-targeted dendritic cell delivery of PLGA-nanoparticle vaccines induce potent anti-tumor responses, Biomaterials 40 (2015) 88–97, https://doi.org/10.1016/j.biomaterials.2014.10.053.
[35] T.N. Alkie, K. Taha-Abdelaziz, N. Barjesteh, J. Bavananthasivam, D.C. Hodgins, S. Sharif, Characterization of innate responses induced by PLGA encapsulated- and soluble TLR ligands in vitro and in vivo in chickens, PLoS One 12 (2017), e0169154, https://doi.org/10.1371/journal.pone.0169154.
[36] S.M. Bal, B. Slütter, R. Verheul, J.A. Bouwstra, W. Jiskoot, Adjuvanted, antigen loaded N-trimethyl chitosan nanoparticles for nasal and intradermal vaccination: adjuvant- and site-dependent immunogenicity in mice, Eur. J. Pharmaceut. Sci. 45 (2012) 475–481, https://doi.org/10.1016/j.ejps.2011.10.003.
[37] A. Haddadi, A. Chaffey, S.H. Ng, D. Yalamati, H.L. Wilson, Combination of innate immune modulators as vaccine adjuvants in mice, Vaccines 8 (2020) 569, https://doi.org/10.3390/vaccines8040569.
[38] C.M. Lundquist, C. Loo, I.M. Meraz, J.D.L. Cerda, X. Liu, R.E. Serda, Characterization of free and porous silicon-encapsulated superparamagnetic iron oxide nanoparticles as platforms for the development of theranostic vaccines, Med. Sci. 2 (2014) 51–69, https://doi.org/10.3390/medsci2010051.
[39] I.M. Meraz, C.H. Hearnden, X. Liu, M. Yang, L. Williams, D.J. Savage, J. Gu, J. R. Rhudy, K. Yokoi, E.C. Lavelle, R.E. Serda, Multivalent presentation of MPL by porous silicon microparticles favors T helper 1 polarization enhancing the anti-tumor efficacy of doxorubicin nanoliposomes, PLoS One 9 (2014), e94703, https://doi.org/10.1371/journal.pone.0094703.
[40] V. Albrecht, T.P. Hofer, B. Foxwell, M. Frankenberger, L. Ziegler-Heitbrock, Tolerance induced via TLR2 and TLR4 in human dendritic cells: role of IRAK-1, BMC Immunol. 9 (2008) 69, https://doi.org/10.1186/1471-2172-9-69.
[41] Invivogen, Pam3CSK4 technical data sheet (n.d.), https://www.invivogen.com/pam3csk4.
[42] Invivogen, Pam3CSK4 Rhodamine Technical Data Sheet, (n.d.).
[43] I. Ramakrishna Rao, Raman effect in water, Nature 125 (1930), https://doi.org/10.1038/125600b0, 600–600.
[44] V.C. Rucker, Detection of DNA by Sequence Specific Fluorescent Polyamides, 2003.
[45] A. Ghafarinazari, M. Scarpa, G. Zoccatelli, M.C. Franchini, E. Locatelli, N. Daldosso, Hybrid luminescent porous silicon for efficient drug loading and release, RSC Adv. 7 (2017) 6724–6734, https://doi.org/10.1039/C6RA27102B.
[46] N. Wang, X. Cheng, N. Li, H. Wang, H. Chen, Nanocarriers and their loading strategies, Adv. Healthcare Mater. 8 (2019), 1801002, https://doi.org/10.1002/adhm.201801002.
[47] D. Liu, L.M. Bimbo, E. Mäkilä, F. Villanova, M. Kaasalainen, B. Herranz-Blanco, C. M. Caramella, V.-P. Lehto, J. Salonen, K.-H. Herzig, J. Hirvonen, H.A. Santos, Co-delivery of a hydrophobic small molecule and a hydrophilic peptide by porous silicon nanoparticles, J. Contr. Release 170 (2013) 268–278, https://doi.org/10.1016/j.jconrel.2013.05.036.
[48] T. Kawasaki, T. Kawai, Toll-like receptor signaling pathways, Front. Immunol. (2014) 5. https://www.frontiersin.org/articles/10.3389/fimmu.2014.00461. (Accessed 2 December 2023).
[49] F. Xing, J. Wang, M. Hu, Y. Yu, G. Chen, J. Liu, Comparison of immature and mature bone marrow-derived dendritic cells by atomic force microscopy, Nanoscale Res. Lett. 6 (2011) 455, https://doi.org/10.1186/1556-276X-6-455.
[50] P. Verdijk, P.A. van Veelen, A.H. de Ru, P.J. Hensbergen, K. Mizuno, H.K. Koerten, F. Koning, C.P. Tensen, A.M. Mommaas, Morphological changes during dendritic cell maturation correlate with cofilin activation and translocation to the cell membrane, Eur. J. Immunol. 34 (2004) 156–164, https://doi.org/10.1002/eji.200324241.